

This is the peer reviewed version of the following article:

There is plenty of asbestos at the bottom. The case of magnesite raw material contaminated with asbestos fibres / Gualtieri, Alessandro F.; Malferrari, Daniele; Di Giuseppe, Dario; Scognamiglio, Valentina; Sala, Orietta; Gualtieri, Magdalena Lassinantti; Bersani, Danilo; Fornasini, Laura; Mugnaioli, Enrico. - In: SCIENCE OF THE TOTAL ENVIRONMENT. - ISSN 0048-9697. - 898:(2023), pp. 1-14.
[10.1016/j.scitotenv.2023.166275]

Terms of use:

The terms and conditions for the reuse of this version of the manuscript are specified in the publishing policy. For all terms of use and more information see the publisher's website.

24/04/2026 16:42

(Article begins on next page)

1 **There is plenty of asbestos at the bottom. The case of magnesite raw**
2 **material contaminated with asbestos fibres**

3

4 Alessandro F. Gualtieri ^{ab}, Daniele Malferrari ^{ab*}, Dario Di Giuseppe ^a, Valentina Scognamiglio ^a,
5 Orietta Sala ^a, Magdalena Lassinantti Gualtieri ^c, Danilo Bersani ^d, Laura Fornasini ^d, Enrico
6 Mugnaioli ^e

7

8 ^a *Department of Chemical and Geological Sciences, University of Modena and Reggio Emilia, Via G. Campi 103,*
9 *41125 Modena, Italy*

10 ^b *Inter-Departmental Research and Innovation Centre on Construction and Environmental Services of the*
11 *University of Modena and Reggio Emilia.*

12 ^c *Department of Engineering "Enzo Ferrari", University of Modena and Reggio Emilia, Via Vivarelli 10, 41125*
13 *Modena, Italy*

14 ^d *Department of Mathematical, Physical and Computer Sciences, University of Parma, Parco Area delle Scienze 7/A*
15 *43124 Parma, Italy*

16 ^e *Department of Earth Sciences, University of Pisa, Via Santa Maria 53 56126 Pisa, Italy*

17

18 *Corresponding author, e-mail: daniele.malferrari@unimore.it

19

20 Science of the Total Environment

21 Submitted as **Research paper**

22

23 **ABSTRACT**

24 Although all six asbestos minerals (the layer silicate chrysotile and five chain silicate species
25 actinolite asbestos, amosite, anthophyllite asbestos, crocidolite and tremolite asbestos) are
26 classified as carcinogenic, chrysotile is still mined and used in many countries worldwide.
27 Other countries, like Italy, impose zero tolerance for all asbestos species, but conflicting views
28 repress the development of globally uniform treaties controlling international trade of
29 asbestos-containing materials. Hence, countries with more severe legislations against the use
30 of these hazardous materials lack of an international safety net against importation of non-
31 compliant products. For the first time, we report the discovery of commercial magnesite raw
32 materials contaminated with white asbestos (chrysotile). X-ray powder diffraction and
33 thermogravimetric/thermodifferential measurements showed the presence of serpentine
34 group minerals in both the semi-processed (powder) and quarried material along with other
35 minerals usually associated with magnesite and serpentine. The univocal identification of
36 chrysotile in the powders was confirmed by its peculiar Raman bands of the OH stretching
37 vibrations between 3500-3800 cm^{-1} , with an intense peak at $\sim 3695 \text{ cm}^{-1}$ and a weak
38 contribution at $\sim 3647 \text{ cm}^{-1}$. Microscopic investigations highlighted the occurrence in all
39 samples of fibres having similar geometric parameters. Transmission electron microscope
40 observations showed that chrysotile forms fibres up to a few microns long and up to 80 nm
41 thick with a nanotube structure characterized by inner channels as large as 30-40 nm. Fibres
42 size analysis obtained by scanning electron microscopy indicates mean length and diameter of
43 5.95 and 0.109 μm with medians of 2.62 and 0.096 μm , respectively; some among the fibres
44 analysed exhibit the so-called "Stanton size" (i.e., asbestos fibres longer than 8 μm and thinner
45 than 0.25 μm that are strongly carcinogenic). Quantitative analysis showed a chrysotile
46 content around 0.01 wt.% not allowed by current regulations in Italy and many other
47 countries.

48 Magnesite is since decades used in countries like Italy for various industrial applications
49 without being aware of the asbestos impurity. More generally, our findings demonstrate that
50 without shared policies aimed at regulating asbestos circulation on the global market,
51 “asbestos-free” national policies will inevitably fail. We call for the revision of global directives
52 on asbestos and implementation of standard analytical protocols for the assessment of
53 asbestos in natural raw materials to never again have another magnesite case.

54

55 *Keywords:* Magnesite, Asbestos, Chrysotile, REACH, Rotterdam Convention, Electron
56 microscopy.

57

58 **1. Introduction**

59 The term “asbestos” refers to the layer-silicate serpentine chrysotile (white asbestos) and
60 five double-chain silicates (amphiboles): actinolite asbestos, amosite (cummingtonite-
61 grunerite asbestos or brown asbestos), anthophyllite asbestos, crocidolite (riebeckite
62 asbestos or blue asbestos) and tremolite asbestos (Case et al., 2011). The International
63 Agency for Research on Cancer (IARC) classifies all the six asbestos species as “carcinogens
64 for humans” (IARC, 2012). Nevertheless, in contrast to the firm position taken by the IARC,
65 only the five amphibole asbestos species are globally banned, and many countries in the
66 world still allow the use of chrysotile (Gualtieri, 2017).

67 International treaties and agreements aimed at regulating the trade of hazardous
68 chemicals, including asbestos, have been stipulated. Due to disagreements over the use of
69 chrysotile and asbestos fibres concentration limits a globally harmonized system is still
70 lacking. Chrysotile remains a mineral of high socio-economic and industrial relevance as in
71 many countries it still represents an important economic resource and its hazardousness is
72 unrecognised or, at the very least, ignored. In addition, even in states where chrysotile has

73 been banned, it is not easy to verify the coupling between government ratification of
74 international conventions and successful enforcement of the ban (Joshi et al., 2006; Lin et al.,
75 2019; Yoon et al., 2018), although feedbacks in many cases are from monitoring activities
76 such as, for example, the implementation of policies for the search for asbestos substitutes,
77 the enforcement of the national surveillance system of the incidence of mesothelioma, and the
78 control over the removal of and its eventual transformation into End-of-Waste (Aryal and
79 Morley, 2020; Chimed-Ochir et al., 2022; Marsili et al., 2017; Thives et al., 2022). In the face of
80 these challenges, it is not surprising that the governing body of the Rotterdam Convention for
81 Hazardous Chemicals has not yet managed to reach consensus for listing chrysotile in Annex
82 III and thus compel producers to label chrysotile. This excellent tool for international trade
83 control of dangerous chemicals is thus not available for chrysotile. It should be remarked that
84 the inclusion of a chemical in the Rotterdam convention requires a unanimous vote of all the
85 countries is needed, and only a handful of supplier or user countries block this.

86 In the European Union, the REACH compliance prohibits any intentional use of asbestos,
87 but allows the presence of category 1A carcinogens, including asbestos fibres, as contaminant
88 in concentrations <0.1wt.% without obligation of labelling. Both the Rotterdam Convention
89 and the REACH compliance are in contrast with more severe domestic laws of some parties
90 like Italy that applies “zero tolerance” (Dl 257/92, 1992) for asbestos fibres; this means that
91 the unauthorised supply, transport, use, including manufacture and handling of asbestos and
92 any material containing asbestos, even in trace, is prohibited. Direct consequences of these
93 legislative disagreements are that asbestos-containing materials (ACMs) may be unknowingly
94 imported and used in countries that have banned all asbestos minerals. An even more
95 complicated situation occurs when asbestos fibres are present as contaminants, perhaps even
96 accidentally. This situation can occur in the exploitation of certain minerals that may contain
97 impurities of naturally occurring asbestos (Gualtieri, 2020).

98 In this scenario, our research group has been working for several years in screening
99 natural raw materials that potentially contains asbestos. Our work is strictly voluntary and
100 motivated by the scientific conviction that only zero exposure of workers and the population
101 is a guarantee for the elimination of asbestos-related health issues. The methodology of this
102 environmental surveillance includes follow-up on reports and notifications from mining
103 companies as well continuous survey of existing literature to uncover cases of raw materials
104 contaminated with asbestos. Knowing the specific rock types and geologic conditions leading
105 to the formation of asbestos, potentially contaminated mineral commodities can be identified.
106 These include Mg-rich silicates like serpentinized olivine (Van Gossen et al., 2003),
107 vermiculite (Addison, 1995; Larson et al., 2010) and many more although, over the years,
108 special concerns have been raised about potential human exposure and risk from asbestos in
109 consumer products containing cosmetic talcum powder, especially its use with infants (Burns
110 et al., 2019; Emory et al., 2020; Finley et al., 2012; Fitzgerald et al., 2019; Gordon et al., 2014;
111 Van Gossen et al., 2003).

112 Hitherto, our activity contributed to disclose the case of a Na-feldspar mined in Orani
113 (Sardinia, Italy) contaminated with asbestos tremolite (Gualtieri et al., 2018) and the case of
114 commercial chrysotile-rich brucite from China, where the use of chrysotile asbestos is allowed
115 (Malferrari et al., 2021). In the case of the Orani feldspar, mined since 1970, the presence of
116 asbestos was discovered in 2015 and the mining activity, in compliance with Italian law, was
117 consequently stopped. Our work contributed to assess unequivocally the nature of the
118 asbestos fibres as tremolite and to recommend a safe selective exploitation of the 'asbestos
119 free' raw material (Gualtieri et al., 2018). In the case of the Chinese brucite (Malferrari et al.,
120 2021), the Italian import flow was promptly halted and the processing sites were cleared,
121 thus avoiding future legal and, most importantly, health complications.

122 Recently we discovered that magnesite (MgCO_3), a widespread industrial raw material,
123 may be contaminated with asbestos. Magnesite is used in several industrial applications such
124 as the production of insulating materials and coatings, as inorganic additive in ceramic inks,
125 pigments and cements, for CO_2 sequestration and as MgO source. This mineral can be
126 associated with serpentine (Tzamos et al., 2020) and eventually also with asbestos minerals
127 when occurring in altered ophiolitic rocks (i.e., outcrops of basic/ultrabasic rocks
128 representing relicts of oceanic crust or upper mantle). In fact, magnesite occurs in four types
129 (Drnek et al., 2018; Pohl, 1990): (i) of sedimentary origin within ancient marine platform
130 carbonate suites (Veitsch type); (ii) in ultramafic magmatic rocks (Kraubath type); (iii) in
131 sedimentary fluviatile-limnic sediments overlying ultramafics (Bela Stena type); (iv) in
132 metamorphosed ultramafics with high magnesite content (Greiner type). Sedimentary type (i)
133 is assumed not to contain asbestos minerals while type (iii) and (iv) are of minor economic
134 importance. On the contrary, the Kraubath type deposits are actively exploited and may
135 contain asbestos minerals formed as a result of lithological transformation processes.

136 In this work, we report the results of a systematic investigation of samples of magnesite
137 from Kraubath type deposits imported from Turkey (KT) and Greece (KG) for use in the
138 Italian production of traditional ceramics. In the title of the paper, we have chosen to
139 paraphrase the famous title of the lecture given by Richard Feynman at the annual American
140 Physical Society meeting in 1959 to point out that asbestos is still among us and circulates in
141 an insidious way. It is essential to bear in mind that magnesite, if uncontaminated, poses no
142 risk. When, on the other hand, it is contaminated with asbestos even at low concentrations, in
143 addition to being illegal in many states, it poses a serious health risk, as shown by the
144 numerous studies on chrysotile toxicity (e.g., [Aryal and Morley, 2020](#); [Gualtieri, 2023, 2020](#);
145 [IARC, 2012](#); [Innes et al., 2021](#); [Lemen and Landrigan, 2017](#)) .

146

147 **2. Materials and Methods**

148

149 *2.1. Samples*

150 Representative samples of magnesite from Kraubath type deposits imported from Turkey
151 (KT) and Greece (KG) and used in Italian manufacture sites of traditional ceramics have been
152 investigated. The samples originate from fine-grained magnesite deposits ([Fig. 1](#)) occurring in
153 veins and stock-works within dunites and peridotites that have undergone serpentinization
154 processes. The Greek magnesite samples come from the Gerakini mining area (Northern
155 Greece) and are located in the magnesite deposits of Chalkidiki Ophiolites complex into the
156 Circum Rhodope Belt which represents low-grade metamorphosed Triassic and Jurassic
157 sedimentary rocks fringing the unified high-grade metamorphic rock of the Hellenic hinterland
158 ([Kauffmann et al., 1976](#); [Meinhold and Kostopoulos, 2013](#)). The Turkish samples are from
159 magnesite deposits occurring in the supra-subduction zone-type ophiolitic complex in the
160 Izmir-Ankara-Erzincan suture zone in northern Anatolia. This area include Paleozoic-Mesozoic
161 metamorphic units, consisting of sericite, schist, glaucophane schist and marble units ([Gozler
162 et al., 1996](#); [Tankut, 1991](#); [Zedef et al., 2000](#)). Further details about the geological description
163 of the two areas can be found in the [Supporting Information \(SI hereafter\) SI-1](#).

164 For this study, both fine powders (KT1 and KG1) and lumps (KT2 and KG2) from the same
165 deposits have been analysed; all the samples were collected from distributors as well as from
166 industrial end-users and the quantity received (about 5 kg) is representative of the batches
167 normally acquired by the company. Initially we were advised of the possible occurrence of
168 chrysotile in the fine powder. Following preliminary investigations that confirmed chrysotile
169 occurrence, massive samples were also taken from companies working with products directly
170 from the quarry before they underwent any kind of processing; in this way, it can be ensured
171 that chrysotile can be traced exclusively to the area of origin. A granulated commercial product

172 of sedimentary Veitsch type from Austria, from now on called VA, was also included in the
173 investigation together with various brands of commercial fine magnesite powders sold by
174 Italian sporting goods retailers as anti-slip agent for various sports activities such as climbing.
175 Among these powders, a commercial hydro-magnesite was also included.

176 Powder samples in most cases were analysed as acquired, while massive samples were
177 pretreated as will be described in the following sections.

178

179 *2.2 X-ray powder diffraction*

180 The mineralogical characterization of the magnesite samples was performed by X-Ray
181 Powder Diffraction (XRPD) using an X'Pert-PRO PANanalytical θ/θ diffractometer (CuK α
182 radiation, 40kV and 40 mA), equipped with a Real Time Multiple Strip detector and Ni filter on
183 the secondary beam. Data were collected from 3 to 80 $^{\circ}2\theta$, with a virtual scan time of 5s/step
184 and step scan of 0.0167 $^{\circ}2\theta$. The XRPD spectra were preliminary analysed using the X-Pert
185 High Score Plus software. A 1/2 $^{\circ}$ divergence slit and a 0.2 mm receiving slit were used. The
186 quantitative mineralogical analysis was performed with the Rietveld method (Rietveld, 1969)
187 using the General Structure Analysis System (GSAS) software package (Larson and Von
188 Dreele, 1994) with the graphical interface EXPGUI (Toby, 2001) and following the protocol
189 reported in Gualtieri et al. (2019). More in detail, XRPD patterns background was modelled
190 using a Chebyshev polynomial of the first kind, peak shapes were modelled using the
191 Thompson–Cox–Hastings pseudo-Voigt function, and March-Dollase function was chosen as
192 intensity correction factor for preferred orientations and applied to the reflections (104) of
193 magnetite and (001) of serpentine. The starting structural models used for the refinement are
194 from Graf (1961) for magnesite, Gualtieri (2000) for quartz, Steinfink and Sans (1959) for
195 dolomite, Ondrus et al. (2003) for calcite, Lister and Bailey (1967) for chlorite and Manceau et

196 al. (1998) for smectite. Lizardite from Mellini (1982) was chosen as the starting structural
197 model for quantitative estimation of serpentine.

198 Samples KT1, KG1 and VA were prepared by mixing randomized samplings and
199 disintegrating them in agata mortar without further grinding. Randomized fragments from
200 KT2 and KG2 samples were previously ground in agate mortar to a fine powder. For all
201 measurements, the powder was placed in the sample holder using side loading to limit
202 preferential grain orientations (Gualtieri et al., 2019).

203

204 *2.3 Thermal analyses and evolved gasses mass spectrometry*

205 Thermogravimetric (TGA) and thermo-differential (DTA) analyses were performed with a
206 Seiko SSC 5200 thermal analyser coupled with quadrupole mass spectrometer (ESS, GeneSys
207 Quadstar 422) to detect gases released during thermal reactions (MSEGA). Gas sampling was
208 done using a silicon capillary pre-heated to avoid gas condensation. Experimental conditions
209 were: heating rate: 20 °C/min; heating range: 25-1000 °C; TGA and DTA data measurement:
210 every 0.5 s; DTA reference: α -alumina powder; purging gas: ultrapure helium with a flow rate
211 of 100 μ L/min. Mass analyses were performed in multiple ion detection mode by measuring
212 m/z ratios (i.e., the dimensionless ratio of the mass number m to the z-charge of an ion) 18,
213 30, 44, 64 to detect the emission of H₂O, NO, CO₂, and SO₂, respectively using a secondary
214 electron multiplier (SEM) detector set at 900 V with 1 s integration time on each measured
215 mass. The samples analysed are the same as those used for XRPD measurements.

216

217 *2.4 Optical microscopy analyses*

218 Preliminary observation of the raw sample (KT2) with A Meiji Techno stereomicroscope
219 (50x) showed that the green veins are characterised by an intergrowth of green plate-like
220 mineral grains with bundles of white mineral fibres with a length between 0.5-0.7 mm. Fibres

221 were gently picked up preserving their morphology using tweezers and subsequently
222 characterised with Phase Contrast Optical Microscope (PCOM). PCOM analyses were
223 conducted following the methodology proposed by Di Giuseppe et al. (2021) for the
224 identification of chrysotile. Analyses were carried out using an Olympus BX51 phase-contrast
225 microscope and Cargille Refractive Index (RI) Liquid $n = 1.550$. Two drops of refractive index
226 medium were placed on a pre-cleaned glass slide (76×26 mm). Few representative fibres or
227 bundles were placed on the slide and covered with a cover slip. PCOM observations were
228 made in both phase contrast and dark field mode. The PCOM technique was not applied to
229 powder magnesite samples due to the small size of the fibres in these samples.

230

231 *2.5 Electron microscopy*

232 The morphological observation of the samples was carried out by a Scanning Electron
233 Microscope (SEM) using JSM-6010PLUS/LA (JEOL, Hillsboro, OR, USA) equipped with an
234 Energy Dispersive X-ray (EDX) microanalysis system (Oxford INCA-350) and Field Emission
235 Gun Scanning Electron Microscope (FEG-SEM) FEI Nova NanoSEM 450 FEG-SEM. The powder
236 sample were investigated as received while small fragments of the raw KT2 and KG2 samples
237 were gently ground in agate mortar to obtain a fine powder. After, according with the Italian
238 Minister Decree 06.09.94 (DM September 06, 1994) the procedure for quantitative SEM
239 analysis was performed as follows: an amount of 5 mg of the sample was suspended in 200 ml
240 of deionized water with 0.1 vol.% surfactant additive (dioctylsodium sulfocinate,
241 $C_{20}H_{37}NaO_7S$, CAS no. 577-11-7), and ultrasonicated for 10 min to promote particle
242 separation. A volume of 6 ml of this suspension was collected at different levels in a becker
243 and placed in a filtration system, allowing random deposition of the particles on
244 polycarbonate filters (20 mm² surface, 0.45 μm porosity). Then the filter was dried at 55 °C
245 and weighed. The final weight of the material deposited on the filter was 0.1 mg. The filter

246 was mounted on an aluminium stub and coated with gold using a Carbon Coater-Balzers CED-
247 010 (10 nm thick). The SEM images were obtained by secondary electron imaging covering 1
248 mm² of surface at 4000× magnification (130 analysis fields).

249 Preliminary TEM investigations focused on the microstructure of the mineral fibres in the
250 samples were carried out at the CIGS-UNIMORE laboratories by using a Talos F200S G2
251 microscope, equipped with S-FEG Schottky field emitter operating at 200 kV and two large-
252 area EDX spectrometers with Silicon Drift Detectors (SDD). Sample preparation almost
253 parallels that described for SEM: small amounts of or gently ground samples KT2 and KG2
254 were suspended with 1 mL of ethanol in a test tube, sonicated for 1 min (using a low power
255 sonic bath) and left to set for 5 min. A drop of the suspension was then transferred and dried
256 onto a 300-mesh carbon copper TEM grid.

257 High resolution transmission electron microscopy (HRTEM), energy-dispersive X-ray
258 spectroscopy (EDS) and three-dimensional electron diffraction (3DED) were performed with
259 a JEOL JEM-F2000 Multi-purpose, working at 200 kV and equipped with Schottky-FEG source
260 and SDD EDS detector. 3DED data were analysed and visualized by ADT3D software (Gemmi
261 et al., 2019; Kolb et al., 2011).

262

263 *2.6 Micro-Raman spectroscopy*

264 The Raman spectra were collected on the magnesite powders (KT1 and KG1) and on a
265 fragment (KT2) with a HORIBA Jobin Yvon LabRam confocal micro-spectrometer (300 mm
266 focal length), using a He-Ne 632.8 nm and a frequency doubled Nd:YAG 473.1 nm laser lines
267 as excitation sources, with an integrated Olympus BX40 microscope with 4×, 10×, 50× ULWD
268 and 100× objectives, a 1800 grooves/mm grating, a XY motorized stage and a Peltier cooled
269 silicon CCD. The spectral resolution is ~2 cm⁻¹ with the 632.8 nm line and ~4 cm⁻¹ with the
270 473.1 nm line. The system was calibrated by using the 520.6 cm⁻¹ Raman peak of silicon in the

271 low-wavenumber spectral region ($100\text{-}1200\text{ cm}^{-1}$) and the emission lines of a gas lamp in the
272 high-wavenumber spectral region ($3000\text{-}4000\text{ cm}^{-1}$). The spectra have been recorded with
273 typical exposures of 60 s repeated at least 4 times. Data analysis has been performed by
274 LabSpec 5 built-in software. Fit with bands deconvolution has been carried out with Gauss-
275 Lorentzian functions. Measurements were performed on the fragment as received, whereas
276 the powders were prepared in a sealed configuration, working in a fume hood. A small
277 amount of powder (a few mg) was stuck to a double-sided tape adhering to a microscope
278 glass. The powder was covered by a coverslip and sealed to the glass substrate. The confocal
279 micro-Raman measurements were carried out by focusing the laser beam on the powder
280 under the coverslip.

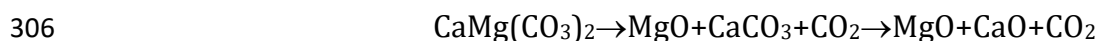
281

282 **3. Results**

283 The XRPD data on the magnesite samples show a number of secondary phases ([Table 1](#)).
284 The mineralogical composition (wt%) of samples KT1 and KG1, performed using Rietveld's
285 quantitative phase analysis ([Fig. 2](#) and [Table 2](#)), revealed magnesite, quartz, serpentine and
286 dolomite in sample KT1, while talc, calcite, smectite and chlorite were also identified in
287 sample KG1.

288 In addition to the magnesite decarbonation, the TGA/DTA-MSEGA analyses highlight, in
289 samples polluted with chrysotile, the typical dehydroxylation reaction of the octahedral sheet
290 of chrysotile followed by an exothermic event indicating its recrystallization in forsterite
291 (Bloise et al., 2016; Cattaneo et al., 2003; Khorami et al., 1984). For both KT1 and KG1, the
292 TGA curves and their first derivative (DTG) show one principal (1) and one minor (2) thermal
293 event, which are both attributed to multiple fully or partially overlapping thermal reactions.
294 An additional thermal event (3) is evidenced by the DTA curve, but only for KT1.

295 In KT1 (Fig. 3a) reaction (1) occurs in the temperature range 445-640 °C (maximum
296 reaction rate at 599 °C) and results in a mass loss of 42.1 wt%. Reaction (2), which occurs
297 between 650 and 735 °C is less evident and produced a mass loss of 1.0 wt%. The DTA curve
298 (Fig. 3b), in addition to the endothermic signals related to reactions (1) and (2), also
299 highlights a weak exothermic reaction (3) with a maximum at about 830 °C. The release of CO₂
300 (m/z=44, Fig. 3c) associated with reaction (1) proves that this thermal event occurs following
301 the decarbonation of magnesite (mainly) and of dolomite (first step). On the other hand,
302 reaction (2) involves the simultaneous release of H₂O (m/z=18, Fig. 3c) and CO₂ that could be
303 respectively related to the dehydroxylation of the serpentine and to the second step of
304 dolomite decarbonation according to the well-known thermal decomposition mechanism
305 (Bloise et al., 2016):



307 where the first step is not distinguishable as completely overlapping with reaction (1).
308 Reaction (3) is due to the recrystallization of the serpentine in forsterite occurring after
309 dehydroxylation (Bloise et al., 2016; Cattaneo et al., 2003; Khorami et al., 1984). Below 250 °C,
310 it is also possible to observe weak reactions, more evident in the magnification of Fig. 3a and
311 in MSEGA curve m/z=18 (Fig. 3c), related to the removal of more or less strongly bound water
312 molecules.

313 The thermal behavior of sample KG1 nearly parallels that of KT1 and is described in the SI-
314 2.

315 Macroscopic fibre bundles were discovered in the raw rock samples. For example, the
316 macroscopic observation of the raw KT2 sample composed of centimetric rock fragments (Fig.
317 4a) shows green lamellar mineral phases and white mineral fibres (L= 0.5–0.7 mm). The latter
318 were selected and observed with PCOM and revealed beautiful bundles of chrysotile fibres
319 (Fig. 4b). The PCOM technique allowed to easily identify the nature of the fibres in KT2. In

320 fact, fibres treated with RI=1.550 liquid displayed the characteristic dispersion colours of
321 chrysotile (Di Giuseppe et al., 2021). Observed in phase contrast mode, fibres colour was light
322 blue with an orange halo when the fibre axis was perpendicular to the polariser, and dark blue
323 with an orange halo when the fibre axis was parallel to the polariser (Fig. 4b).

324 The SEM images of raw and powder magnesite samples from Turkey (KT1, KT2) and
325 Greece (KG1, KG2) show a matrix of massive magnesite particles with several flexible bundles
326 of chrysotile fibres (Fig. 5a-d) whose nature has been confirmed by the EDX analyses (Fig. 5
327 e,f). A series of representative SEM images were analysed using *ImageJ* software, which
328 provides accurate measurements of the length and width of the chrysotile fibre. Data,
329 resumed in Table 3 and reported in detail in SI-3 show that fibres observed in the Turkish and
330 Greek samples are characterized by very close geometrical parameters; analysis of the size
331 distribution shows that most of the fibres have lengths between 0 and 15 (Figure SI-3a) μm
332 and diameters between 0.05 and 0.2 μm (Figure SI-3b). Therefore, many fibres, regardless of
333 whether they are from powder (KT1 and KG1) or massive (KT2 and KG2) samplings display
334 the so-called "Stanton size": based on *in vivo* animal studies, asbestos fibres longer than 8 μm
335 and thinner than 0.25 μm are strongly carcinogenic and induce malignant pleural
336 mesothelioma (Stanton et al., 1981; Stanton and Wrench, 1972). The quantitative SEM
337 analysis carried out according to the Italian Ministry of Health regulations and technical
338 methodologies (DM September 06, 1994) highlighted a chrysotile content of 0.012 wt.% for
339 KT1 (0.012 wt.% for KT2 and 0.010 wt.% for the KG samples).

340 TEM observations confirm that chrysotile is the fibrous phase present in the investigated
341 Turkish and Greek magnesite samples. In particular, sample KT2 contains fibres long up to
342 few microns and thick up to 80 nm (Fig. 6a). A closer look reveals that these fibres have a
343 nanotube structure, with internal channels that may be more or less visible and large up to
344 30-40 nm (Fig. 6b). More massive fragments are also present in the KT2 sample, although

345 with a significantly lower incidence. EDS measurements show that both fibres and massive
346 fragments have a comparable composition, consistent with serpentine minerals (Fig. 6c).
347 3DED analysis confirms that the fibres are chrysotile; the reconstructed diffraction volume
348 shows typical crowns of diffuse scattering produced by the bending of the serpentine layers
349 (Fig. 6d). 3DED also reveals that massive fragments consist of lizardite or polygonal
350 serpentine; the latter is easily recognizable due to the circular crowns of reflections arranged
351 according to a pseudo five-fold symmetry (Fig. 6e) (Baronnet et al., 1994). All the other
352 samples consist mostly of magnesite crystals of different size. Elongated tubular fibres are
353 also spotted very frequently. Some fibres display a habit similar to the chrysotile detected in
354 sample KT2, but the most common form consists of bent hair-like fibres typically arranged in
355 crowded bundles (see for example the chrysotile fibres in sample KG2 reported in Fig. 6f).

356 The Micro-Raman data confirm the results obtained with the other experimental
357 techniques. The signal of chrysotile was detected in both Turkish and Greek samples. In the
358 Turkish powder KT1, lizardite was also observed, and its signal sometimes appears in
359 conjunction with that of chrysotile. In the low-wavenumber spectral range, the Raman signals
360 related to the lattice vibrational modes and the internal vibration of the SiO₄ tetrahedra of a
361 serpentine phase were observed in KT1 (at 229, 385, 619, 690 cm⁻¹) and in KG1 (at 392, 689
362 cm⁻¹) (Fig. 7a). The contribution of magnesite from the surrounding crystals was also detected
363 (at 211, 329, 738, 1094 cm⁻¹) (Fig. 7a). The univocal identification of chrysotile in the powders
364 was confirmed by its peculiar Raman bands of the OH stretching vibrations (Fornasini et al.,
365 2022), between 3500-3800 cm⁻¹, with an intense peak at ~3695 cm⁻¹ and a weak contribution
366 at ~3647 cm⁻¹ (Fig. 7b). Typically, the most intense peak of chrysotile is also characterized by
367 a shoulder at ~3680 cm⁻¹, which is markedly pronounced in KT1. A possible contribution due
368 to lizardite, in addition to chrysotile, may explain this curve shape, since its most intense OH
369 stretching signal occurs at 3683 cm⁻¹ (Auzende et al., 2004; Petriglieri et al., 2015). The

370 presence of chrysotile in KT1 was supported by the analysis on the raw fragment (KT2),
371 whose Raman spectrum corresponds to that of chrysotile (characteristic peaks occurring at
372 233, 391, 691 and 1104 cm^{-1} in the low-wavenumber range and at 3697 with a shoulder at
373 $\sim 3687 \text{ cm}^{-1}$ in the OH stretching region).

374

375 **4. Discussion**

376 Our systematic investigation clearly shows that a small amount of chrysotile is present as
377 the only asbestos phase in the Kraubath type industrial minerals from Greece and Turkey. The
378 Austrian granulate of sedimentary Veitsch type (VA) as well the powders sold at retail as anti-
379 slip agent do not contain asbestos at all. We rule out the possibility of contamination during
380 materials processing of the industrial minerals as chrysotile fibres were found in both the
381 powders and the raw fragmented rocks. It should be stressed that even small amounts of
382 asbestos such as those we have highlighted pose a risk as a direct consequence of the large
383 number of fibres they may release.

384 Only the use of a suite of different experimental techniques made it possible to assess
385 indisputably that chrysotile is present in these magnesite products. In this context, XRPD and
386 TGA/DTA are inconclusive methods while micro-Raman and electron microscopy techniques
387 are decisive for revealing the true crystal-chemical nature of the fibres. Fine powders are
388 particularly challenging and high-resolution electron microscopy analyses of carefully
389 prepared specimens are indispensable for revealing the presence of fibre bundles. Hence,
390 even actors in the supply chain that have actively searched for asbestos contaminants may
391 have failed due to inadequate analysis methods. Together with the lack of adequate and
392 shared analytical protocols, this could be a reason why chrysotile was not revealed before by
393 the magnesite producers.

394 In Italy, this magnesite product has been used as raw material in the traditional ceramics
395 industry for decades without being aware of the asbestos contaminant. Our discovery reveals
396 major flaws in the global network and a number of violations and conflicts. Regarding the
397 violations, asbestos contaminated magnesite should be considered as illicit in countries like
398 Italy, Germany and France where the marketing of all ACMs, with a few exceptions, where
399 banned during the 90s (Décret 96-1133, 1996; dlg 257/92, 1992; Gesetz 162, 1993). This
400 applies also to industrial minerals where asbestos has not been intentionally added even in
401 very low concentration. There is also a violation of the 2009 European directive (EC
402 2009/148, 2009) on the protection of workers from the risks related to exposure to asbestos
403 at work as *“Even though it has not yet been possible to identify the exposure threshold below*
404 *which asbestos does not involve a cancer risk, occupational exposure to workers to asbestos*
405 *should be reduced to a minimum.”* Another violation regards the fact that, according to the
406 2006 EU Regulation (EC 2006/1907, 2006), all articles containing asbestos must bear the
407 “asbestos” label. Unfortunately, a number of conflicts and discrepancies make the actual
408 situation chaotic. The 2006 EU Regulation specifically prohibits the placing on the market of
409 articles and mixtures containing asbestos fibres *“added intentionally”*. Because chrysotile is
410 not added intentionally to magnesite but is a natural contaminant, is this “article” out of the
411 2006 EU Regulation? The same Regulation admits a content of carcinogens, including
412 asbestos, of 0.1 wt%. In this case, the Turkish magnesite powder (KT1) for example, with a
413 chrysotile content of 0.012 wt.%, would be legal in the EU.

414 Regarding importation from extra-EU countries, the Rotterdam convention is a precious
415 tool for the adhering parties (including EU countries) in avoiding accidental importation of
416 domestically forbidden substances. In fact, the Rotterdam Convention deals with *“substances*
417 *whether by itself or in a mixture ...”* (Article 1) with no specification of the quantity except for a
418 generic statement on *“...chemicals in quantities not likely to affect human health...”* (Article 3);

419 the latter, however, is not the case though because it is well known that there is no evidence
420 for a threshold or a “safe” level of asbestos exposure (see for example, Lemen and Landrigan,
421 2017). Each party is obliged to guarantee that exporters within its jurisdiction do not ship
422 listed chemical to other parties that disapproves importation of them. This multilateral treaty
423 regulates the international trade of hazardous chemicals, listed in Annex III to the convention.
424 Whereas amphibole asbestos species are listed, chrysotile is still only recommended for
425 listing by the Chemical Review Committee. The outcome is that legal responsibilities shift
426 from exporters to importers, with an obvious increased risk of finding non-compliant
427 products on the European market. Hence, in countries like Italy, asbestos contaminated
428 magnesite is automatically out of law only when it is already present in its territory.

429 This chaos in the global market of ACMs has negative consequences for countries that
430 wish to protect people from any exposure to asbestos fibres. For example, workers handling
431 industrial raw materials containing unknown asbestos contaminants do not make adequate
432 use of protective measures and the exposure risk increases (Burdett and Bard, 2007; Douglas
433 and Van den Borre, 2019); moreover and it is not possible to predict when this will happen
434 since this risk is not affected by any seasonality. The Individual companies can suffer from
435 severe economic losses and legal issues if the presence of ACMs is discovered by the local
436 environmental/health authorities. The site can be impounded by a state’s attorney with the
437 suspension of the working activity and access prohibited until the end of the legal action. This
438 was the case with the Italian feldspar mine contaminated with tremolite asbestos (Gualtieri et
439 al., 2018).

440 It is sad to acknowledge that countries (like Italy) hardly targeting to turn “asbestos-
441 free” (Terracini, 2019) or at least “asbestos-safe” see their efforts thwarted by the income of
442 new contaminated materials on their territory without their knowledge.

443

444 5. Conclusions

445 The global use of asbestos is decreasing worldwide (Frank and Joshi, 2014) but is still
446 not zero. Naturally occurring asbestos (Gualtieri, 2020) is another threat to the public health
447 that transforms from local to geographically widespread when the fibres are present as
448 impurity in industrial minerals that may freely circulate among states seriously impacting the
449 total environment. The magnesite case reported here is a perfect example of this type of
450 situation and proves that there is still plenty of asbestos at the bottom. Our research group
451 will continue the screening of commercial raw materials in search of asbestos for predictive
452 purposes. We have to avoid *ex post* discovering of the exposure of the population or workers
453 to some mineral source through the observation of malignant mesothelioma morbidity peaks
454 as was the case in the past for fluoro-edenite in Biancavilla (Italy) (Comba et al., 2003) or
455 fibrous erionite in Cappadocia (Turkey) (Baris et al., 1987).

456 In concrete terms, we believe that without a global ban of asbestos (Douglas and Van
457 den Borre, 2019), which appears to be utopic at the moment, only shared harmonized policies
458 aimed at regulating asbestos mining and circulation adopted by all the countries that have
459 banned asbestos and that aspire to become asbestos-free can drive us to see the light at the
460 end of the tunnel. We call for a harmonized standard analytical protocol: when imported, each
461 raw material and especially those of asbestos-compatible origin, must be accompanied by a
462 certification of absence of asbestos phases, assessed by a suite of analytical determination
463 including not only chemical and diffractometric investigations, but also high-resolution SEM
464 or TEM, that producers (the mining companies) deliver. The importing company/national
465 distributors can randomly cross-check the reliability of the certificates by validated
466 specialized labs using the analytical methodologies described here in detail for the magnesite
467 case. Although it is realistic that zero risk cannot be achieved by avoiding false negatives, we
468 believe that by proceeding analytically as proposed here, it can be approached considerably.

469 Following the instance of the talc mining industry (Schlossman, 2009) and the example of
470 New Caledonia where the exploitation of serpentine rocks contaminated by asbestos is strictly
471 regulated (Worliczek, 2017), mining activity in asbestos-rich or supposedly asbestos-rich
472 national deposits should be always carried out under severe monitoring and differential
473 processing to avoid exploitation of asbestos-rich levels. As for the case above, the domestic
474 distribution of the raw materials delivered to the production sites must be accompanied by a
475 certification of absence of asbestos phases.

476 The conflict between the European REACH compliance (EC 2006/1907, 2006) that
477 admits a content of carcinogens, including asbestos, of 0.1 wt% in circulating raw materials,
478 and the national laws must be resolved by making an exception for asbestos in the list of
479 REACH carcinogens so that, compatible with the SEM experimental detection limits, the raw
480 materials should not contain asbestos phases.

481 Finally, at a global level, we call for the inclusion of chrysotile in the list of Rotterdam
482 convention of Hazardous Chemicals under the Rotterdam Convention to be labelled for
483 import/export operations.

484

485 **CRedit authorship contribution statement**

486 Alessandro F. Gualtieri: Supervision, Project administration, Conceptualization, Resources,
487 Formal analysis, Methodology, Validation, Writing the original draft, Writing, review and
488 editing, Funding acquisition. Daniele Malferrari: Supervision, Methodology, Validation,
489 Writing, review and editing, Funding acquisition. Dario Di Giuseppe: Investigation, review and
490 editing. Valentina Scognamiglio: Investigation, review and editing. Orietta Sala: Investigation,
491 review and editing. Magdalena Lassinantti Gualtieri: Conceptualization, Writing the original
492 draft, Writing, review and editing. Danilo Bersani: Investigation, Writing – review and editing.

493 Laura Fornasini: Investigation, Writing – review and editing. Enrico Mugnaioli: Investigation,
494 Writing – review and editing.

495

496 **Acknowledgments**

497 The work is supported by the PRIN project fund “Fibres: a multidisciplinary mineralogical,
498 crystal-chemical and biological project to amend the paradigm of toxicity and cancerogenicity
499 of mineral fibres” (PRIN: Progetti di Ricerca di Rilevante Interesse Nazionale—Bando 2017—
500 Prot. 20173X8WA4). Authors thanks the Center for Instrument Sharing of the University of
501 Pisa (CISUP), Italy, for the TEM measurements.

502

503 **Data availability**

504 Data will be made available on request.

505

506 **Declaration of competing interest**

507 The authors declare that they have no known competing financial interests or personal
508 relationships that could have appeared to influence the work reported in this paper.

509

510 **References**

511 LA COMPONGO CON ZOTERO A REVISIONE CONCLUSA

512

513 **Figure captions**

514

515 **Fig. 1.** (a) Distribution of Tethyan ophiolites along Alpine-Himalayan suture zone (modified
516 from Lippard et al., 1986); (b) Focus of main geotectonic units and suture zones of NE Greece

517 and NW Turkey, with magnesite KT and KG localization samples (modified from Meinhold and
518 Kostopoulos, 2013).

519

520 **Fig. 2.** Graphical output of the Rietveld refinement of KT1 (a) and KG1 (b) powder samples.
521 Red crosses represent the observed pattern, the thin green line represents the calculated
522 pattern, and the blue bottom line is the difference line. The vertical bars mark of the peaks of
523 each crystalline phase included in the refinement procedure which are (from the bottom):
524 magnesite, dolomite, serpentine and quartz (a); magnesite, dolomite, serpentine, quartz, talc,
525 chlorite, calcite and smectite (b).

526

527 **Fig. 3.** Thermal behaviour of samples KT1. (a) TGA (solid lines) and DTG (dashed lines)
528 curves; (b) DTA curve (the maxima denote exothermic reactions); (c) MSEGAs for H₂O
529 (m/z=18) and CO₂ (m/z=44); the curves for NO (m/z=30) and SO₂ (m/z=64) are not reported
530 as these gasses were not detected.

531

532 **Fig. 4.** Macroscopic (a) and microscopic (b) observation of KT2 sample. (a) KT2 sample occurs
533 as centimetric fragments of grey-white rock with green veins (I); a magnification of the area
534 marked by the white arrow in (I) shows that the green veins are characterised by an
535 intergrowth of green plate-like mineral grains with white mineral fibre bundles highlighted by
536 the white arrows (II). (b) Chrysotile fibres observed with PCOM in bright (I) and (II) and dark
537 (III) and (IV) field. Fibres perpendicular to the polarizer, in bright field, have pale blue colour
538 and orange halo (I); fibres parallel to the polarizer, in bright field, have dark blue colour and
539 orange halo (II); fibres perpendicular to the polarizer, in dark field, have blue colour (III);
540 fibres parallel to the polarizer, in dark field, have purple colour (IV). The images (III) and (IV)

541 show the Walton-Beckett graticule (100 μm in diameter) to identify the length and width of
542 the fibres.

543

544 **Fig. 5.** Representative SEM images of Turkish and Greek magnesite samples: (a) flexible
545 chrysotile bundle with frayed and split ends dipped in a matrix of massive magnesite particles
546 in sample KT1; (b) detail of chrysotile fibres in magnesite fragments presents in sample KG1;
547 (c) elongated fibrous bundle with split ends in sample KT2; (d) detail of chrysotile fibres
548 dipped in a matrix massive magnesite particle in sample KG2; (e-f) representative EDX
549 spectra of the chrysotile fibres and magnesite particles shown in (a) and (b), respectively.

550

551 **Fig. 6.** Representative TEM images of the magnesite samples KT2 (a-e) and KG2 (f). (a) High-
552 angle annular dark-field images of chrysotile fibres; (b) A chrysotile fibre with a particularly
553 large channel of about 40 nm in diameter; (c) Massive fragments with composition, consistent
554 with serpentine minerals; (d) Reconstructed 3DED volume showing typical crowns of diffuse
555 scattering produced by the bending of the serpentine layers to form chrysotile; (e)
556 Reconstructed 3DED data set from a massive polygonal serpentine; (f) Examples of bent hair-
557 like fibres typically arranged in bundles.

558

559 **Fig. 7.** Raman spectra of KT1, KG1 and KT2 in the low-wavenumber (a) and in the OH-
560 stretching (b) spectral regions.